DR. LUCAS CAMPOS CURCINO VIEIRA (Orcid ID : 0000-0002-1138-9117)

Article type : Research Article

Rational Design, Synthesis and Evaluation of Indole Nitrogen Hybrids as Photosystem II Inhibitors

Jéssica Maria de Souza[1], Bruno Rodrigues Fazolo[1], Jhully Wellen Ferreira Lacerda[1], Mariana de Souza Moura[1], Arielly Celestino Rodrigues dos Santos[1], Leonardo Gomes de Vasconcelos[1], Paulo Teixeira de Sousa Junior[1], Evandro Luiz Dall'Oglio[1], Akbar Ali[2], Olívia Moreira Sampaio[1], Lucas Campos Curcino Vieira*[3]

[1] Department of Chemistry, Federal University of Mato Grosso, Cuiabá, 78060-900, Brazil

[2] Department of Chemistry, University of Malakand, 18800, Pakistan

[3] Engineering Faculty, Federal University of Mato Grosso, Várzea Grande, 78060-900, Brazil

*Corresponding author e-mail: lucascurcino@ufmt.br (Lucas Campos Curcino Vieira)

ABSTRACT

We report the synthesis of twelve indole derivatives bearing nitro or amide groups via Fischer indole methodology followed by reduction/acetylation and amidation reactions. After thorough characterization these indoles were subjected to a number of studies in order to evaluate their bioactive potential as photosynthesis and plant growth inhibitors. Firstly, these molecular hybrids were evaluated as photosystem II (PSII) inhibitors through chlorophyll *a* (Chl *a*) fluorescence measurement. In this study, 6-Chloro-8-nitro-2,3,4,9-tetrahydro-1*H*-carbazole (**15a**) and 5-chloro-2,3-dimethyl-7-nitro-1*H*-indole (**15b**) showed the best results by reducing the phenomenological parameters of reaction centres ABS/RC, TR_0/RC and ET_0/RC of PSII. Electron chain blockage by these compounds may lead to diminished ATP synthesis and CO_2 fixation which interrupt the plant development. The compounds **15a** and **15b** both act as post-emergent herbicides, reducing the dry biomass of *Ipomoea grandifolia* and *Senna alata* weeds average of 40% and 37%, respectively, corroborating the fluorescence results. Additionally, the molecular docking study revealed that the presence of strong electron withdrawing groups at the indole phenyl ring are important for the ligand's interaction with the binding pocked of protein D1 on PSII. The optimization of these molecular features is the goal of our research group in further understanding and development of new potent herbicides.

INTRODUCTION

Herbicides are a pesticide class that affect several plant physiological processes, including metabolic energy transfer, which inhibit plant development and growth. Among the most common effects of herbicides on plant physiology are the photosynthetic apparatus stress on photosystem II (PSII) and plant growth inhibition (1–3). In last few years, weed control in agriculture has been carried out principally via the use of herbicides. Continual and repetitive use of herbicides leads to increased occurrence of herbicide-resistant weeds as well as continuous damage to the environment and to human health, making the development of novel, environmentally benign herbicidal agents for the replacement of currently commercialized herbicides an indispensable area of research (4–8).

Intensive efforts aimed at developing new herbicidal compounds or modifying existing ones are ongoing (9–16). A wide variety of chemical compounds have demonstrated plant management activity including the indole derivatives **1** and **2** (12) which demonstrate photosynthesis inhibitory activity as well as compounds **3** (17) and **4** (18) which are plant growth inhibitors (Fig. 1).

<Figure 1>

In addition to privileged scaffolds such as indole, the presence of electron donating and/or withdrawing groups may improve the herbicidal activity by modifying physicochemical properties such as molecular size, hydrogen bonding, ionization state, lipophilicity and aqueous solubility (19, 20). In this context, compounds bearing nitro or amide groups have demonstrated improved herbicidal activity compared to unfunctionalized adducts. Compounds containing nitro groups have been studied as photosynthesis inhibitors, for example compound **5,** which is an inhibitor of carbon dioxide fixation (21) as well as compound **6**, which blocks electron transport at the quinone B level by interacting at the D1 protein (22). In addition, the commercial herbicides pendimethalin (**7**) and trifluralin (**8**) inhibit root and shoot growth (23, 24). Furthermore, herbicidal activity has been reported for a number of amide derivatives as photosynthetic electron transport inhibitors (**9-11**) (25–27) as well as for naptalam (**12**) which inhibits both basipetal auxin transport and root elongation (Fig. 1) (28).

The development of new herbicides based on molecular hybridization is an important strategy, particularly when the active hybrid molecules possess independent modes of action (29–32). Molecular hybridization is a rational strategy to develop new prototypes based on the fusion of two bioactive compounds and also the chemical modification of bioactive molecules. This method provides new molecules which might present improved activity relative to the original molecule the activities of both parent molecules expressed in a single hybrid structure (33–37).

Our aims in this work are the synthesis of an array of indole derivatives containing amide or nitro groups (Fig. 1), evaluation and determination of the effects of these compounds on photosynthetic apparatus and plant development through root and stems growth and dry biomass assays.

MATERIALS AND METHODS

General Information. Unless otherwise noted, all commercially available reagents were purchased from Aldrich Chemical Co. and used without purification. Column chromatography was performed using Merck Silica Gel (230-400 mesh). Thin layer chromatography (TLC) was performed using Merck Silica Gel GF254, 0.25 mm thickness. For visualization, TLC plates were either placed stained with iodine vapor or acidic vanillin. Nuclear magnetic resonance (^{1}H NMR) spectra and (^{13}C NMR) spectra were recorded on a Bruker 500 MHz Nuclear Magnetic Resonance. The coupling constants (J) are given in hertz (Hz) and chemical shifts are denoted in parts per million (ppm) downfield from internal standard, tetramethylsilane (TMS). The abbreviations s, bs, d, t, q, m, and dd refer to singlet, broad singlet, doublet, triplet, quartet, multiplet, and doublet of doublets, respectively. All NMR spectra were obtained with $CDCl_3$ or DMSO-*d*6. Fourier transform infrared spectroscopy (FTIR) analysis was performed on Shimadzu Iraffinity-1 Spectrophotometer. KBr pellets were prepared mixing the compounds (1 mg) with pure and anhydrous KBr (100 mg). The high resolution mass spectra (HRMS) data were recorded on UFLC/DAD/MicroTOF.Melting points were recorded on a PFM-II / MS Tecnopon melting point apparatus.

*General Method for the Synthesis of Compounds **14a-b***. A solution of substituted phenyl amine (**13a-b**) (0.16 mol) in HCl 37% (6.5 mL) was cooled to 0˚C. To the resulting cooled solution was added sodium nitrite (7.24 mmol in 4.0 mL water) dropwise under stirring at the same temperature and stirred for 10 min. Subsequently, a solution of $SnCl_2.2H_2O$ (0.026 mol in 3.5 mL HCl 37%) was added dropwise. Then, the resulting suspension was stirred at 0 ˚C for 30 min. The resulting residue was filtered, washed with diethyl ether (2 × 10 mL) and dried under vacuum. The crude product was used for further reactions without purification (38).

*General Method for the Synthesis of Compounds **15a-d***. Using a modified literature procedure (39), to a suspension of substituted phenylhydrazine hydrochloride (**14a-b**) (1.50 mmol) and cyclohexanone or 2-butanone (1.50 mmol) in water (8 mL) was added H_2SO_4 (0.7 mmol). The mixture was heated at 100˚C for 30 min. After completion of the reaction, the mixture was cooled to room temperature and cold water (10 mL) was added. The precipitate was filtered, washed with water (3 x 10 mL) and dried under reduced pressure to provide the hydrazone intermediate.

To a suspension of hydrazone intermediate in acetic acid (8 mL) was added $ZnCl_2$ (0.01 mol, 1.36 g). The mixture was heated at 118ºC for 12 h. After completion of the reaction, the mixture was cooled to 0°C, the precipitate was filtered off, washed with cold water (10 mL) and dried under reduced pressure to provide the crude product. Further purification was achieved by flash column chromatography on a silica gel employing hexane:ethyl acetate (9:1) to give the desired products.

6-chloro-8-nitro-2,3,4,9-tetrahydro-1H-carbazole **(15a).** Yield: 32% (120 mg). Orange solid. Melting point: 212 ºC (lit.: 215 ºC) (40). **IR** (KBr pellet, cm^{-1}): 3417, 2931, 2846, 1512. **NMR ^{1}H** (DMSO-d_6, 500 MHz) δ: 1.76-1.85 (m, 4H), 2.62-2.64 (m, 2H), 2.76-2.78 (m, 2H), 7.88 (d, J = 1.8 Hz, 1H), 7.91 (d, J = 1.91 Hz, 1H). **NMR ^{13}C** (DMSO-d_6, 125 MHz) δ: 20.0, 22.3, 22.8, 110.0, 116.0, 121.8, 124.4, 126.8, 131.5, 132.7, 140.6.

5-chloro-2,3-dimethyl-7-nitro-1H-indole **(15b).** Yield: 30% (101 mg). Orange solid. Melting point: 201-205 ºC (lit.: 202 ºC) (40). **IR** (KBr pellet, cm^{-1}): 3387, 3093, 2924, 2854, 1512, 1365, 1307, 1296, 894. **NMR ^{1}H** (DMSO-d_6, 500 MHz) δ: 2.17 (s, 3H), 2.39 (s, 3H), 7.91 (d, J = 1.9 Hz, 1H),

7.93 (d, J = 1.8 Hz, 1H), 11.67 (br s, 1H). **NMR ^{13}C** (DMSO-d_6, 125 MHz) δ: 8.40, 11.70, 107.82, 116.54, 122.34, 125.21, 126.92, 131.90, 134.86, 138.24.

8-chloro-6-nitro-2,3,4,9-tetrahydro-1H-carbazole (15c). Yield: 44% (165 mg). Yellow solid. Melting point: 220-225 ºC (lit.: 218 ºC) (40). **IR** (KBr pellet, cm^{-1}): 3348, 2931, 2854, 1512, 1481, 1327, 1296, 887. **NMR ^{1}H** (DMSO-d_6, 500 MHz) δ: 1.78-1.87 (m, 4H), 2.67-2.70 (m, 2H), 2.74-2.76 (m, 2H), 7.94 (d, J = 1.9 Hz, 1H), 8.30 (d, J = 1.9 Hz, 1H), 11.87 (br s, 1H). **NMR ^{13}C** (DMSO-d_6, 125 MHz) δ: 20.70, 22.78, 22.84, 23.17, 113.14, 113.76, 115.19, 115.61, 128.16, 136.02, 140.66.

7-chloro-2,3-dimethyl-5-nitro-1H-indole **(15d):** Yield: 36% (121 mg) Yellow solid. Melting point: 245-248 ºC (lit.: 230 ºC) (40). **IR** (KBr pellet, cm^{-1}): 3348, 3093, 2924, 2854, 1519, 1481, 1327, 887. **NMR ^{1}H** (DMSO-d_6, 500 MHz) δ: 2.22 (s, 3H), 2.36 (s, 3H), 7.93 (d, J = 1.98 Hz, 1H), 8.33 (d, J = 1,98 Hz, 1H), 11.84 (br s, 1H). **NMR ^{13}C** (DMSO-d_6, 125 MHz) δ: 8.14, 11.19, 109.88, 113.53, 114.59, 114.90, 129.24, 135.01, 137.26, 140.21.

General Method for the Synthesis of Compounds ***16a-d:*** Using modified literature procedures (41, 42), to a solution of nitro derivative (**15a-d**) (0.20 mmol) in ethyl acetate (3 mL) was added $SnCl_2.2H_2O$ (1.4 mmol, 0.316 g). The mixture was stirred at room temperature for 48 h. After completion of the reaction, an NH_4OH solution (2 mL) was added, and the precipitate was filtered and washed with ethyl acetate (3 x 10 mL). The organic layers were combined and the solvent was removed under reduced pressure to provide amine intermediate.

To a solution of the amine intermediate in acetic acid (3.0 mL) was added acetic anhydride (10.6 mmol, 1.00 mL) and 10% aqueous solution of sodium acetate (6.0 mL). The mixture was stirred at room temperature for 4 h. After completion of the reaction, water (10 mL) was added to the mixture and extracted with dichloromethane (2 x 5.0 mL). The organic layers were combined, washed with saturated aqueous solution of $NaHCO_3$, brine and solvent was removed under reduced pressure. Further purification was achieved by flash column chromatography on a silica gel employing hexane:ethyl acetate (1:2) to give the desired products.

***N-(6-chloro-2,3,4,9-tetrahydro-1H-carbazol-8-yl)acetamide* (16a):** Yield: 24% (12 mg). Purple solid. Melting point: 230 ºC. **IR** (KBr pellet cm^{-1}): 3317, 2931, 2854, 1651, 1535, 1481, 1411, 725. **NMR ^{1}H** (DMSO-d_6, 500 MHz) δ: 1.75-1.85 (m, 4H), 2.12 (s, 3H), 2.56-2.58 (m, 2H), 2.71-2.73 (m, 2H), 7.13 (d, J = 1.7 Hz, 1H), 7.47 (d, J = 1.8 Hz, 1H), 9.64 (s, 1H), 10.49 (s, 1H). **NMR ^{13}C** (DMSO-d_6, 125 MHz) δ: 20.39, 22.64, 22.73, 23.73, 108.75, 112.10, 112.58, 122.39, 123.74, 125.81, 129.09, 135.80, 168.41. **HR-ESI-MS**: $C_{14}H_{16}ClN_2O$ $[M+H]^+$ *m/z* found 263.0958, calculated 263.0951.

***N-(5-chloro-2,3-dimethyl-1H-indol-7-yl)acetamide* (16b):** Yield: 35% (18 mg). Green solid. Melting point: 254-260 ºC. **IR** (KBr pellet, cm^{-1}): 3294, 2924, 2854, 1658, 1535, 1465, 1373, 894. **NMR ^{1}H** (DMSO-d_6, 500 MHz) δ: 2.10 (s, 3H), 2.11 (s, 3H), 2.31 (s, 3H), 7.14 (d, J = 1.84 Hz, 1H), 7.46 (d, J = 1.83 Hz, 1H), 9.62 (br s, 1H), 10.47 (br s, 1H). **NMR ^{13}C** (DMSO-d_6, 125 MHz) δ: 8.21, 11.24, 23.76, 105.83, 111.93, 112.75, 122.39, 123.51, 125.30, 130.73, 132.74, 168.44. **HR-ESI-MS**: $C_{12}H_{14}ClN_2O$ $[M+H]^+$ *m/z* found 237.0799, calculated: 237.0795.

***N-(8-chloro-2,3,4,9-tetrahydro-1H-carbazol-6-yl)acetamide* (16c):** Yield: 38% (20 mg). Grey solid. Melting point: 290-295 ºC. **IR** (KBr pellet, cm^{-1}): 3294, 3116, 2931, 2854, 1658, 1558, 1450, 1381, 864. **NMR ^{1}H** (DMSO-d_6, 500 MHz) δ: 1.76-1.81 (m, 4H), 2.00 (s, 3H), 2.54-2.56 (m, 2H), 2.67-2.69 (m, 2H), 7.33 (d, J = 1.68 Hz, 1H), 7.48 (d, J = 1.52 Hz, 1H), 9.78 (br s, 1H), 10.84 (br s, 1H). **NMR ^{13}C** (DMSO-d_6, 125 MHz) δ: 20.59, 22.63, 22.77, 22.81, 23.88, 106.64, 109.30, 112.64, 114.25, 128.66, 129.13, 131.54, 136.98, 167.71. **HR-ESI-MS**: $C_{14}H_{16}ClN_2O$ $[M+H]^+$ *m/z* found 263.0968, calculated 263.0951.

***N-(7-chloro-2,3-dimethyl-1H-indol-5-yl) acetamide* (16d):** Yield: 26% (17 mg). Blue solid. Melting point: 210 ºC. **IR** (KBr pellet, cm^{-1}): 3209, 3078, 2924, 2854, 1627, 1581, 1489, 894, 717. **NMR ^{1}H** (DMSO-d_6, 500 MHz) δ: 2.01 (s, 3H), 2.09 (s, 3H), 2.30 (s, 3H), 7.32 (d, J = 1.54 Hz, 1H), 7.50 (d, J = 1.32 Hz, 1H), 9.79 (br s, 1H), 10.84 (br s, 1H). **NMR ^{13}C** (DMSO-d_6, 125 MHz) δ: 8.41, 11.15, 23.88, 106.30, 106.83, 112.58, 113.97, 128.64, 130.20, 131.50, 133.93, 167.69. **HR-ESI-MS**: $C_{12}H_{13}ClN_2NaO$ $[M+Na]^+$ *m/z* found 259.0662, calculated 259.0614.

*General Method for the Synthesis of Compounds **20a-b***. Using a modified literature procedure (43), to a solution of compounds **19a** or **19b** (0.7 mmol) in ethanol (5 mL) was added dropwise H_2SO_4 (5.72 mmol, 0.305 mL). The mixture was refluxed for 16 h. After completion of the reaction, water (10 mL) was added to the mixture and extracted with diethyl ether (3 x 10 mL). The organic layers were combined, washed with saturated aqueous solution of $NaHCO_3$ (3 x 10 mL), brine and the solvent removed under reduced pressure. Further purification was achieved by flash column chromatography on a silica gel employing hexane:ethyl acetate (9:1) to give the desired products.

Ethyl 2,3,4,9-tetrahydro-1H-carbazole-8-carboxylate **(20a):** Yield: 70%. White solid. Melting point: 84-85 ºC (lit.: 76 ºC).(43) **IR** (KBr pellet, cm^{-1}): 3402, 2985, 1674, 1265. **NMR ^{1}H** (DMSO-d_6, 500 MHz) δ: 1.42 (t, J = 7.17 Hz, 3H), 1.84-1.94 (m, 4H), 2.69-2.71 (m, 2H), 2.75-2.77 (m, 2H), 4.42(q, J = 7.17 Hz, 2H), 7.07 (t, J = 7.63 Hz, 1H), 7.63 (d, J = 7.63 Hz, 1H), 7.78 (d, J = 7.63 Hz, 1H), 9.39 (br s, 1H). **NMR ^{13}C** (DMSO-d_6, 125 MHz) δ: 14.46, 20.80, 23.11, 23.19, 23.20, 60.59, 109.97, 111.81, 118.18, 122.94, 123.10, 129.02, 135.37, 135.80, 167.80.

Ethyl 2,3-dimethyl-1H-indole-7-carboxylate **(20b):** Yield: 62%. White solid. Melting point: 144-146 ºC (lit.: 104-106 ºC).(44) **IR** (KBr pellet, cm^{-1}): 3402, 2978, 1674, 1265. **NMR ^{1}H** (DMSO-d_6, 500 MHz) δ: 1.43(t, J = 7.15 Hz, 3H), 2.23 (s, 3H), 2.39 (s, 3H), 4.43 (q, J = 7.15 Hz, 2H), 7.08 (t, J = 7.61 Hz, 1H), 7.85 (d, 7.77 Hz, 1H), 7.78 (dd, J = 7.61 and 0.9 Hz, 1H), 9.39 (s, 1H). **NMR ^{13}C** (DMSO-d_6, 125 MHz) δ: 8.36, 11.54, 14.45, 60.57, 106.92, 111.55, 118.10, 122.88, 123.30, 130.62, 131.94, 135.32, 167.77.

*General Method for the Synthesis of Compounds **21a-b.*** Modified literature procedure (45), a suspension of **20a** or **20b** (0.206 mmol), 40% aqueous CH_3NH_2 (0.600 mL) in ethanol (1 mL) was stirred at r.t. for 5 days. After completion of the reaction, the mixture was extracted with ethyl acetate (3 x 10 mL). The organic layers were combined, washed with brine and the solvent removed under reduced pressure. Further purification was achieved by flash column chromatography on a silica gel employing dichloromethane:methanol (95:5) to give the desired products **21a** or **21b**.

N-methyl-2,3,4,9-tetrahydro-1H-carbazole-8-carboxamide **(21a):** Yield: 19%. White solid. Melting point: 224-225 ºC. **IR** (KBr pellet, cm^{-1}): 3394, 3309, 3055, 1643. **NMR ^{1}H** (DMSO-d_6, 500 MHz) δ: 1.84-1.93 (m, 4H), 2.69-2.71 (m, 2H), 2.74-2.77 (m, 2H), 3.04 (s, 3H), 6.36 (br s, 1H), 7.03 (t, J = 7.63 Hz, 1H), 7.23 (dd, J = 0.6 and 7.48 Hz, 1H), 7.58 (dd, J = 0.6 and 7.79 Hz, 1H), 9.83 (s, 1H). **NMR ^{13}C** (DMSO-d_6, 125 MHz) δ: 20.96, 23.24, 23.32, 23.39, 26.60, 109.56, 115.07, 117.69, 118.03, 121.66, 129.57, 135.39, 136.10. 168.97. **HR-ESI-MS**: $C_{14}H_{17}N_2O$ $[M+H]^+$ *m/z* found 229.1347, calculated 229.1341.

N,2,3-trimethyl-1H-indole-7-carboxamide **(21b):** Yield: 21%. White solid. Melting point: 190-193 ºC. **IR** (KBr pellet, cm^{-1}): 3441, 3325, 2954, 1620. **NMR ^{1}H** (DMSO-d_6, 500 MHz) δ: 2.22 (s, 3H), 2.37 (s, 3H), 3.04 (s, 3H), 6.33 (br s, 1H), 7.04 (t, J = 7.63 Hz, 1H), 7.22 (dd, J = 0.46 and 7.48 Hz, 1H), 7.59 (d, J = 7.48 Hz, 1H), 9.82 (br s, 1H). **NMR ^{13}C** (DMSO-d_6, 125 MHz) δ: 8.50, 11.67, 26.57, 106.53, 114.81, 117.64, 117.96, 121.87, 131.20, 132.73, 134.93, 168.96. **HR-ESI-MS**: $C_{12}H_{15}N_2O$ $[M+H]^+$ *m/z* found 203.1186, calculated 203.1184.

Chlorophyll a fluorescence measurements (semi in vivo assay). According to a modified literature procedure (12), ten spinach leaves were cut into 1.0 cm diameter discs and placed with 20 mL of modified Krebs solution into a Petri dish (9 cm diameter), the solution consisted of NaCl (115 mM), KCl (5.9 mM), $MgCl_2$ (1.2 mM), KH_2PO_4 (1.2 mM), Na_2SO_4 (1.2 mM), $CaCl_2$ (25 mM), and $NaHCO_3$ (25 mM, pH = 7.4). After 12 h of incubation at room temperature, compounds **15a-d**, **16a-d**, **20a-b** and **21a-b** were added in dimethyl sulfoxide (DMSO) solutions at 100 μM for each Petri dish and incubated for 6 additional hours. Then, the discs were adapted in the dark for 30 min. Finally, chlorophyll *a* (Chl *a*) fluorescence transients were measured using a Hansatech Handy- Plant Efficient Analyzer; a three LEDs array allowed for illumination with 650 nm continuous light. DMSO was used as negative control in order to consider the solvent effect. OJIP transients were analysed according to the JIP test (see Supporting Information). The experiment was performed in triplicate and the results were expressed as mean and standard error.

Plant material for in vivo assays. Commercially available seeds of *Ipomoea grandifolia*, *Senna alata* and *Sida rhombifolia* weeds were placed in plastic pots (top diameter, 10.5 cm; bottom diameter,

7.5 cm; height, 7.0 cm) filled with approximately 100 g of a mixture of 80:20 w/w soil/vermiculite (plant growth medium). All pots were watered every day, maintained in a greenhouse at 25-30°C and under normal day/night illumination. Plants were selected by uniformity size after 20 days of growth *S. rhombifolia* and 4 days for *I. grandifolia* and *S. alata*. Plants of similar size were separated in three groups: negative control (DMSO), positive control (DCMU) and experimental treated with compounds **15a-b** and **21b** at 50 and 100 μM

Determination of Chl a fluorescence in intact leaves. Chl *a* fluorescence was measured in leaves of the control plant and those treated with compounds **15a-b** and **21b** at 50 and 100 μM. After 1 h and 72 h of treatment, the plants adapted in the dark for 30 min were excited by light from an array of three light-emitting diodes delivering 3000 μmol m^{-2} s^{-1} of red light (650 nm). The Chl *a* fluorescence induction curves were measured at room temperature with a portable Hansatech Fluorescence Handy PEA (plant efficiency analyser) apparatus.

Plant growth assay. To evaluate the effect of **15a-b** and **21b** in *I. grandifolia*, *S. alata* and *S. rhombifolia* plant growth, the plant length and dry biomass was measured after 10 days of treatment. Dry biomass was determined by drying all components in an oven at 60˚C for 15 days. Negative and positive controls were performed using DMSO and DCMU, respectively. PDW was measured using an analytical balance (2).

Molecular docking. Molecular docking simulations were performed to analyse interactions of the compounds **15a-d**, **16a-d**, **20a-b** and **21a-b** with the active site of spinach photosystem II (PDB deposited code: 3JCU) using the AutoDock 4.2 software (46). Chemical structures of the ligands were drawn in the ChemDraw Professional 15.0 software followed by MM2 energy minimization.

According to a modified procedure (47), the target enzyme was prepared for molecular docking using the chain A of the protein, followed by removal of all water molecules, addition of all hydrogens, Gasteiger charges calculations, and lastly, all nonpolar hydrogens were merged to carbon atoms. A grid box size of 40 × 40 × 40 points in x, y and z directions and -41.788, 3.115, -18.728 grid centre was set for the enzyme. The box was centred based on the cognate ligand with a spacing of 0.486 Å. Cluster

analysis was performed on the docked results using a root mean square deviation (RMSD) tolerance of 2 Å (48). The genetic algorithm with local search (GALS) was used to find the best conformers. The Lamarckian genetic algorithm with default settings was used as well. Each docking experiment was iterated 100 times, yielding 100 docked conformations. Best docking pose was selected on the basis of key interacting residues: cluster RMS, number of hydrogen bonds and minimum binding energy.

PyMOL software (PyMOL Molecular Graphics System, Version 1.8 Schrödinger, LLC) was employed to show binding pose of indole derivatives in protein D1 (see Supporting Information).

Statistical analysis. Chl *a* fluorescence measurement (PI_{abs} parameter) and plant growth assays were performed in a completely randomized design. Data were analysed by means of analysis of variance (ANOVA), and treatment means were compared by Tukey test (Honestly significant differences, HSD) (5 and 1 %) was used to estimate least significant range between means (12).

RESULTS AND DISCUSSION

Indole derivative synthesis

The synthesis of nitro-indole derivatives **15a-d** was based on Fischer indole methodology. Substituted anilines (**13a-b**) were diazotized employing sodium nitrite in hydrochloric acid followed by the reduction of the resultant diazonium chloride salts using stannous chloride in hydrochloric acid to furnish **14a-b** in a good yields (38). Aqueous solutions of phenyl hydrazine hydrochlorides **14a-b** were refluxed with cyclohexanone or 2-butanone in the presence of sulfuric acid to provide the hydrazone intermediates, which were reacted with $ZnCl_2$ in acetic acid to afford indoles **15a-d** (39). Then, the nitro groups were reduced employing $SnCl_2.2H_2O$ and thereafter acetylation reaction with acetic anhydride provides the amide derivatives **16a-d** (Scheme 1) (41, 42).

<Scheme 1>

To obtain compounds **21a-b**, the carboxylic acid derivatives **19a-b** (12) were refluxed in ethanol using sulfuric acid as catalyst providing the ester derivatives **20a-b** in moderate to good chemical yields (43). Thus, compounds **20a-b** were reacted with methylamine aqueous solution to furnish the amide derivatives **21a-b** (Scheme 2) (45).

<Scheme 2>

Effect of indole derivatives on Chl *a* fluorescence transient

Semi in vivo assays. The performance index per absorption (PI_{abs}) has been considered the most sensitive parameter for plant stress detection on PSII (49), relating the efficiency of excitation energy absorption, electron capture and transfer by PSII, providing valuable information about environmental stress on the photosynthetic apparatus (50–52). Almost all of the investigated hybrid molecules showed appreciable activity decreasing PI_{abs} parameter on Chl *a* fluorescence (Fig. 2).

<Figure 2>

The lowest values for PI_{abs} were obtained when the leaf discs were exposed to **15a-b** and **21b** ($p < 0.01$). Nitro-indole derivatives **15a-d** reduced PI_{abs} parameter from 40% to 56%, however the conversion of the nitro to an amide group (**16a-d**) decreased the inhibitory activity and there was no statistically significant difference among them compared to the control ($p > 0.05$). The amides **21a-b** showed better inhibitory activity than the corresponding esters **20a-b**, which increased PI_{abs} by 13% and 16%, respectively.

Additionally, the reduction of the parameters related to the reaction centre (RC) such as energy fluxes for absorption (ABS/RC), electron trapping (TR_0/RC), electron transport (ET_0/RC) and energy dissipation (DI_0/RC) as well as the quantum yield parameters ($PHI(P_0)$, PSI_0 and $PHI(E_0)$) corroborate the inhibitory activity on PSII (Fig. 3) (49).

<Figure 3>

The plant physiological vitality can be evaluated through the variation of PI_{abs} and V_j fluorescence parameters, which can corroborate the compound activity on active site of PSII.(52) The J-level increase (2 ms) is characteristic of the transient OJIP fluorescence curve that describes the effects of compounds by blocking the electron transport chain on PSII beyond the Q_A site. The indole derivatives **15a-b** and **21b** at 50 μM and 100 μM increased the V_j parameter by 100% to 150%, confirming the blockage of electron passage in the quinone pool, which corresponds to the Q_A re-oxidation kinetics by electron transfer to Q_B (53).

Compound **15a** reduced ET_0/RC, PSI_0 and PHI(E_0) by 30%, 20% and 25%, respectively, at 50 μM and 100 μM (Fig. 3**(**A)). This variation shows the electron flow blockage through the transport chain, indicating that PSII active reaction centres become heat sinks or silent reaction centres because the energy is not employed to reduce Q_A (54). Compound **15b** demonstrated better results at 50 μM reducing TR/RC, ET_0/RC and PHI(E_0) parameters by 20%, 34% and 22%, respectively (Fig. 3 (B)). This decrease shows the absorbed energy was trapped, reducing the electron flow in active reaction centres. Additionally, the PsbS protein of the photosystem II increases the thermal dissipation of the energy absorbed by the photosystem (52).

Compound **21b** demonstrated the best result by blocking the electron flow. The ABS, TR_0, ET_0, and DI_0 parameters by RC were reduced by 38%, 38%, 52% and 37% respectively, at 100 μM (Fig.3 (C)). The energy absorption reduction by the antenna complex directly influences the electron transport and system energy dissipation, resulting in the photosynthesis Z-scheme not occurring properly (55). The decrease of PSI_0 and PHI(E_0) parameters by 30% and 35%, respectively corroborating the reduction of PSII quantum efficiency by these compounds, suggesting a decrease in electron excitation and transfer by the electron transport chain after Q_A^-.

In vivo assays. Compounds **15a-b** and **21b** which showed the best activity in *semi in vitro* assays were evaluated in *in vivo* experiments employing *Ipomoea grandifolia*, *Senna alata* and *Sida rhombifolia*

weeds at 50 μM and 100 μM. The effects of **15a-b** and **21b** on PI_{abs} parameter were evaluated after 1 and 72 hours after treatment with the active compounds (Fig. 4 (A-C)).

<Figure 4>

All compounds impacted the photosynthetic apparatus over the course of the experiment. The effects of indole derivatives on *I. grandifolia* and *S. alata* plants were observed only after 72 hours of treatment, potentially due to aspects of the plant's physiology which increase the time taken by the bioactive compounds to reach the PSII on the thylakoid membrane. The best results against *I. grandifolia* were observed with compounds **15b** and **21b** at 50 μM, which decreased the PI_{abs} parameter by 20% and 11%, respectively. In the *S. alata* assay, compounds **15a-b** at 50 μM reduced PI_{abs} parameter by 18% and 19%, respectively. The improved activity observed of compounds **15b** (ClogP 3.954) and **21b** and (ClogP 1.991) compared to **15a** (ClogP 4.577) at low concentration can be rationalized by the reduced lipophilicity coefficient (ClogP), as the ClogP increases, water solubility of the compound is decreased, which affects the biological activity.

The PI_{abs} parameter was decreased by an average of 77% to 87% by compounds **15a-b** and **21b** at both concentrations after 1 hour of treatment for *S. rhombifolia* plant. However, after 72 hours of treatment, PI_{abs} parameter increased by an average of 44% to 136% compared to control. These results are related to the low photosynthetic capacity and initial stress adaptation caused by the indole derivatives, indicating the efficiency of the photosynthetic process in the plant is impacted by reversible stress effects on PSII (16).

The effects of **15a-b** and **21b** on photosynthetic quantum parameters in *I. grandifolia*, *S. alata* and *S. rhombifolia* plants are displayed in Fig. 5. In *I. grandifolia* plants (Fig. 5 (A)), compounds **15b** and **21b** reduced ET_0/RC, $PHI(E_0)$, PSI_0 and $(PHI(P_0)$ parameters by an average of 10%. The electron transport and quantum yield reductions suggest an interruption of the photosynthesis process. Additionally, the lower maximum quantum yield of the primary photochemistry and the electron transport chain after Q_A^- indicates that the effect was at the quinone pool on the acceptor side of PSII.

The increase of DI_0/RC and V_j parameters by 15% and 20% respectively, corroborate the electron flow blockage described previously, due to an excess of energy being dissipated in a non-photochemical way and that the detrimental effect was at the polyphasic level J (2 ms) in the quinone redox process.

<Figure 5>

Compounds **15a-b** showed the best results against *S. alata* plants (Fig. 5 (B)), at 50 μM after 72 hours of treatment. Compounds **15a** and **15b** decreased the phenomenological parameters by reaction centre ABS/RC, TR_0/RC and ET_0/RC by an average of 25% and 10%, respectively. The electron transport chain blockage on PSII was confirmed by the action site location through an increase of V_j parameter by 28% (**15a**) and 18% (**15b**).

Compounds **15a-b** and **21b** showed appreciable results on *S. rhombifolia* plants after 1 hour of contact and completely lost their activity after 72 h, potentially due to a self-protection mechanism of the *S. rhombifolia* weed by the stressed conditions induced by the compound (Fig. 5 (C)). The indole derivatives showed similar activity on PSII, increasing ABS/RC, TR_0/RC and DI_0/RC parameters by an average of 17% to 31%, 10% to 18% and 32% to 56%, respectively, demonstrating that the compounds lead to inhibition of the Q_A redox process via energy accumulation in reaction centres. The reduction of quantum parameters PHI(E_0), PSI_0 and PHI(P_0) by 22%-40%, 17%-34% and 10%, respectively, confirm the electron transport chain was affected in the primary photochemical process leading to an accumulation of Q_A^- at PSII.

The effects caused by **15a-b** and **21b** in the *in vivo* studies are not significant compared to the *semi in vivo* assay. Compound penetration into the living plant is impeded by several factors, including membrane permeability, compound solubility, subcellular compartmentalization, and a number of complicating physiological process. These can completely overturn *in vivo* inhibitory activity for a given compound (56).

Effect of indole derivatives on plant growth

The phytotoxic activity of **15a-b** and **21b** was evaluated through plant growth assays employing *I. grandifolia*, *S. alata* and *S. rhombifolia* weeds. Plant length and dry biomass were evaluated after 6 days of treatment with **15a-b** and **21b** at 50 μM and 100 μM. DMSO was used as negative control and DCMU was employed as positive control at 50 μM (Fig. 6).

<Figure 6>

All active compounds showed same behaviour; decreasing plant length and dry biomass, except for the *S. rhombifolia* weed which showed no variation in plant growth (Fig. 6 (C)).

On the *I. grandifolia* weed (Fig. 6 (A)), indole derivative **15a** showed the best results at 100 μM reducing the plant length and dry biomass by 24% and 40%, respectively. Compound **21b** decreased plant length by 30% and dry biomass by 31% at 50 μM and 100 μM, respectively. Compound **15b** affected the plant growth by reducing the plant length by 30% at 100 μM; however, the dry biomass was not reduced.

These results suggest that the photosynthesis inhibitory activity diminishes the synthesis of ATP and CO_2 fixation which disturbs plant development. The best result was achieved for **15b** in *S. alata* at 50 μM which demonstrated a similar activity to commercial herbicide DCMU, reducing the dry biomass by 37% at 50 μM compared to the control (Fig.6 (B)). These results corroborate the PSII inhibitory activities demonstrated by the Chl *a* fluorescence assay, indicating that **15a** and **15b** have a selective action as a post-emergent herbicide, blocking the electron transfer process at PSII in the plants. These compounds appear to be potential herbicides with similar symptoms such as chlorosis and necrosis of the plant tissue exhibited by the photosynthesis inhibitor as with DCMU.

Molecular docking

The docking was carried out for all synthesized compounds employing the protein D1 of the PSII reaction centre from *Spinacia oleracea* (PDB ID: 3JCU). In addition, herbicides that inhibit PSII prefer the position near the loop made by Ser264 and Phe265 at protein D1. The same orientation for indole derivatives and DCMU in the binding site was observed (57–59). Figure 7 exhibits the best docking pose of compounds **15a** and **15b** including hydrogen bonding interactions, with binding energies of -8.47 kcalmol^{-1} and -7.39 kcalmol^{-1}, respectively.

<Figure 7>

The nitro group of **15a-d** forms strong hydrogen bond interactions with the OH group of Ser264 and the NH group of His252 with an individual bond-length range of 1.799–1.971Å. These hydrogen-bonding interactions play a key role in determining the 3D space position of the nitro derivatives in the binding pocket of protein D1. Additionally, hydrophobic interactions were observed with Phe211, Met214, His215, Leu218, Val219 and Leu271. For compounds **15c** and **15d**, the exchange of a nitro for a chlorine group on the indole scaffold disfavours hydrogen bonds and hydrophobic interactions at the protein D1 active site, reducing their binding energies to -7.62 kcalmol^{-1} and -6.82 kcalmol^{-1}, respectively.

In this pocket, the amide group of compounds **16a-d** acts as hydrogen bond acceptor with the backbone OH of Ser264 and the imidazole NH of His252. Furthermore, the amide group acts as an electron donating group, increasing the indole ring's electron density, disfavouring Pi-sigma interactions with the residues Leu218 and Leu271, decreasing the affinity with the binding site. The difference observed between the binding mode of the ester derivatives **20a-b** and amide derivatives **21a-b** is associated to the strong hydrogen-bonding interaction that the amide group of **21a-b** forms in the site pocket with His252, with a distance bond of 1.888 Å for **21b**.

These results suggest that hydrogen bond acceptors and electron withdrawing groups on the indole phenyl ring are important for ligand interactions via hydrogen bond formation with Ser264 and

His252 as well as the hydrophobic interactions with Leu218 and Leu271, potentially leading to an inhibition of protein D1 on PSII.

CONCLUSION

This work demonstrates the synthesis of indole derivatives based on the principle of molecular hybridization and their evaluation as photosynthesis and plant growth inhibitors. The best results were obtained for the compounds 6-chloro-8-nitro-2,3,4,9-tetrahydro-1*H*-carbazole (**15a**) and 5-chloro-2,3-dimethyl-7-nitro-1*H*-indole (**15b**), which decreased the phenomenological parameters ABS/RC, TR_0/RC and ET_0/RC of PSII. The compound **15a** and **15b** act as the post-emergent herbicide prototype since the dry biomass was reduced through plant growth assays employing *I. grandifolia*, *S. alata* and *S. rhombifolia* weeds. The best result was achieved for **15b** in *S. alata* at 50 μM which demonstrated similar activity to commercial herbicide DCMU reducing the dry biomass by 37% at 50 μM compared to the control, corroborating the fluorescence results.

The nitro indole derivatives showed better results than amide indole derivatives indicating the presence of strong electron withdrawing groups at indole phenyl ring is important for the ligand's interaction with the binding pocked of protein D1 on PSII as showed by molecular docking studies. Moreover, optimization of these molecular features is a goal of our group in further understanding and development of new herbicides.

ACKNOWLEDGEMENTS- This work has been supported in part by FAPEMAT (grant 0217830/2017 and 0250685/2017), CNPq (grant 430089/2016-3) and UFMT for financial support and fellowships. This study was financed in part by the Coordenação de Aperfeiçoamento de Pessoal de Nível Superior - Brasil (CAPES) - Finance Code 001.

SUPPORTING INFORMATION

Additional supporting information may be found online in the Supporting Information section at the end of the article:

Table S1. Formulae and explanation of the technical data of the OJIP curves and the selected JIP-test parameters used in this work.

Table S2. Binding interaction of indole derivatives (**15a-d**, **16a-d**, **20a-b** and **21a-b**) and DCMU with the pocket site of PSII of *Spinacia oleracea L.*, and ClogP.

Figure S1. Models of the binding interaction of **15a** with the pocket site of PSII of *Spinacia oleracea* (PDB ID: 3JCU).

Figure S2. Models of the binding interaction of **15b** with the pocket site of PSII of *Spinacia oleracea* (PDB ID: 3JCU).

Figure S3. Models of the binding interaction of **15c** with the pocket site of PSII of *Spinacia oleracea* (PDB ID: 3JCU).

Figure S4. Models of the binding interaction of **15d** with the pocket site of PSII of *Spinacia oleracea* (PDB ID: 3JCU).

Figure S5. Models of the binding interaction of **16a** with the pocket site of PSII of *Spinacia oleracea* (PDB ID: 3JCU).

Figure S6. Models of the binding interaction of **16b** with the pocket site of PSII of *Spinacia oleracea* (PDB ID: 3JCU).

Figure S7. Models of the binding interaction of **16c** with the pocket site of PSII of *Spinacia oleracea* (PDB ID: 3JCU).

Figure S8. Models of the binding interaction of **16d** with the pocket site of PSII of *Spinacia oleracea* (PDB ID: 3JCU).

Figure S9. Models of the binding interaction of **20a** with the pocket site of PSII of *Spinacia oleracea* (PDB ID: 3JCU).

Figure S10. Models of the binding interaction of **20b** with the pocket site of PSII of *Spinacia oleracea* (PDB ID: 3JCU).

Figure S11. Models of the binding interaction of **21a** with the pocket site of PSII of *Spinacia oleracea* (PDB ID: 3JCU).

Figure S12. Models of the binding interaction of **21b** with the pocket site of PSII of *Spinacia oleracea* (PDB ID: 3JCU).

Figure S13. Models of the binding interaction of **DCMU** with the pocket site of PSII of *Spinacia oleracea* (PDB ID: 3JCU).

Figure S14. ^{1}H NMR spectrum of compound **15a** (DMSO-$_{d6}$, 500 MHz).

Figure S15. ^{13}C NMR spectrum of compound **15a** (DMSO-$_{d6}$, 125 MHz).

Figure S16. ^{1}H NMR spectrum of compound **15b** (DMSO-$_{d6}$, 500 MHz).

Figure S17. ^{13}C NMR spectrum of compound **15b** (DMSO-$_{d6}$, 125 MHz).

Figure S18. ^{1}H NMR spectrum of compound **15c** (DMSO-$_{d6}$, 500 MHz).

Figure S19. ^{13}C NMR spectrum of compound **15c** (DMSO-$_{d6}$, 125 MHz).

Figure S20. ^{1}H NMR spectrum of compound **15d** (DMSO-$_{d6}$, 500 MHz).

Figure S21. ^{13}C NMR spectrum of compound **15d** (DMSO-$_{d6}$, 125 MHz).

Figure S22. ^{1}H NMR spectrum of compound **16a** (DMSO-$_{d6}$, 500 MHz).

Figure S23. ^{13}C NMR spectrum of compound **16a** (DMSO-$_{d6}$, 125 MHz).

Figure S24. ^{1}H NMR spectrum of compound **16b** (DMSO-$_{d6}$, 500 MHz).

Figure S25. ^{13}C NMR spectrum of compound **16b** (DMSO-$_{d6}$, 125 MHz).

Figure S26. ^{1}H NMR spectrum of compound **16c** (DMSO-$_{d6}$, 500 MHz).

Figure S27. ^{13}C NMR spectrum of compound **16c** (DMSO-$_{d6}$, 125 MHz).

Figure S28. ^{1}H NMR spectrum of compound **16d** (DMSO-$_{d6}$, 500 MHz).

Figure S29. ^{13}C NMR spectrum of compound **16d** (DMSO-$_{d6}$, 125 MHz).

Figure S30. ^{1}H NMR spectrum of compound **20a** ($CDCl_3$, 500 MHz).

Figure S31. ^{13}C NMR spectrum of compound **20a** ($CDCl_3$, 125 MHz).

Figure S32. ^{1}H NMR spectrum of compound **20b** ($CDCl_3$, 500 MHz).

Figure S33. ^{13}C NMR spectrum of compound **20b** ($CDCl_3$, 125 MHz).

Figure S34. ^{1}H NMR spectrum of compound **21a** ($CDCl_3$, 500 MHz).

Figure S35. ^{13}C NMR spectrum of compound **21a** ($CDCl_3$, 125 MHz).

Figure S36. ^{1}H NMR spectrum of compound **21b** ($CDCl_3$, 500 MHz).

Figure S37. ^{13}C NMR spectrum of compound **21b** ($CDCl_3$, 125 MHz).

REFERENCES

1. Green, J. M. (2014) Current state of herbicides in herbicide-resistant crops. *Pest Manag. Sci.* **70**, 1351–1357. https://doi.org/10.1002/ps.3727.

2. Sampaio, O. M., Lima, M. M. de C., Veiga, T. A. M., King-Díaz, B., da Silva, M. F. das G. F. and Lotina-Hennsen, B. (2016) Evaluation of antidesmone alkaloid as a photosynthesis inhibitor. *Pestic. Biochem. Physiol.* **134**, 55–62. https://doi.org/10.1016/j.pestbp.2016.04.006.

3. Sampaio, O., Vieira, L., Bellete, B., King-Diaz, B., Lotina-Hennsen, B., da Silva, M., Veiga, T., Sampaio, O. M., Vieira, L. C. C., Bellete, B. S., King-Diaz, B., Lotina-Hennsen, B., Da Silva, M. F. das G. F. and Veiga, T. A. M. (2018) Evaluation of Alkaloids Isolated from Ruta graveolens as Photosynthesis Inhibitors. *Molecules* **23**, 2693. https://doi.org/10.3390/molecules23102693.

4. Bałczewski, P., Biczak, R., Turek, M., Pawłowska, B., Różycka-Sokołowska, E., Marciniak, B., Deska, M. and Skalik, J. (2018) Ammonium 2,2′-thiodiacetates – Selective and environmentally safe herbicides. *Ecotoxicol. Environ. Saf.* **163**, 408–416. https://doi.org/https://doi.org/10.1016/j.ecoenv.2018.07.093.

5. Dinehart, S. K., Smith, L. M., McMurry, S. T., Anderson, T. A., Smith, P. N. and Haukos, D. A. (2009) Toxicity of a glufosinate- and several glyphosate-based herbicides to juvenile amphibians from the Southern High Plains, USA. *Sci. Total Environ.* **407**, 1065–1071. https://doi.org/https://doi.org/10.1016/j.scitotenv.2008.10.010.

6. Hoagland, R. E., Boyette, C. D., Weaver, M. A. and Abbas, H. K. (2007) BIOHERBICIDES: RESEARCH AND RISKS. *Toxin Rev.* **26**, 313–342. https://doi.org/10.1080/15569540701603991.

7. Saha, S., Dutta, D., Karmakar, R. and Ray, D. P. (2012) Structure–toxicity relationship of chloroacetanilide herbicides: Relative impact on soil microorganisms. *Environ. Toxicol. Pharmacol.* **34**, 307–314. https://doi.org/https://doi.org/10.1016/j.etap.2012.04.014.

8. Federico, C., Motta, S., Palmieri, C., Pappalardo, M., Librando, V. and Saccone, S. (2011) Phenylurea herbicides induce cytogenetic effects in Chinese hamster cell lines. *Mutat. Res. Toxicol. Environ. Mutagen.* **721**, 89–94. https://doi.org/https://doi.org/10.1016/j.mrgentox.2010.12.013.

9. Ye, F., Zhai, Y., Kang, T., Wu, S.-L., Li, J.-J., Gao, S., Zhao, L.-X. and Fu, Y. (2019) Rational design, synthesis and structure-activity relationship of novel substituted oxazole isoxazole carboxamides as herbicide safener. *Pestic. Biochem. Physiol.* **157**, 60–68. https://doi.org/https://doi.org/10.1016/j.pestbp.2019.03.003.

10. Hernández-Romero, Y., Acevedo, L., de Los Ángeles Sánchez, M., Shier, W. T., Abbas, H. K. and Mata, R. (2005) Phytotoxic Activity of Bibenzyl Derivatives from the Orchid Epidendrum rigidum. *J. Agric. Food Chem.* **53**, 6276–6280. https://doi.org/10.1021/jf0508044.

11. Rios, M. Y., Córdova-Albores, L. C., Ramírez-Cisneros, M. Á., King-Díaz, B., Lotina-Hennsen, B., León Rivera, I. and Miranda-Sánchez, D. (2018) Phytotoxic Potential of Zanthoxylum affine and Its Major Compound Linarin as a Possible Natural Herbicide. *ACS Omega* **3**, 14779–14787. https://doi.org/10.1021/acsomega.8b02020.

12. Mendes, M. C. da S., Fazolo, B. R., De Souza, J. M., De Vasconcelos, L. G., De Sousa Junior, P. T., Dall'Oglio, E. L., Soares, M. A., Sampaio, O. M. and Vieira, L. C. C. (2019) Synthesis and evaluation of indole derivatives as photosynthesis and plant growth inhibitors. *Photochem. Photobiol. Sci.* **18**, 1350–1358. https://doi.org/10.1039/c8pp00506k.

13. Zhang, Y.-Y., Gao, S., Liu, Y.-X., Wang, C., Jiang, W., Zhao, L.-X., Fu, Y. and Ye, F. (2020) Design, Synthesis, and Biological Activity of Novel Diazabicyclo Derivatives as Safeners. *J. Agric. Food Chem.* **68**, 3403–3414. https://doi.org/10.1021/acs.jafc.9b07449.

14. Zhao, L.-X., Jiang, M.-J., Hu, J.-J., Zou, Y.-L., Cheng, Y., Ren, T., Gao, S., Fu, Y. and Ye, F.

(2020) Design, Synthesis, and Herbicidal Activity of Novel Diphenyl Ether Derivatives Containing Fast Degrading Tetrahydrophthalimide. *J. Agric. Food Chem.* **68**, 3729–3741. https://doi.org/10.1021/acs.jafc.0c00947.

15. Ye, F., Zhai, Y., Guo, K.-L., Liu, Y.-X., Li, N., Gao, S., Zhao, L.-X. and Fu, Y. (2019) Safeners Improve Maize Tolerance under Herbicide Toxicity Stress by Increasing the Activity of Enzymes in Vivo. *J. Agric. Food Chem.* **67**, 11568–11576. https://doi.org/10.1021/acs.jafc.9b03587.

16. Digrado, A., De La Motte, L. G., Bachy, A., Mozaffar, A., Schoon, N., Bussotti, F., Amelynck, C., Dalcq, A. C., Fauconnier, M. L., Aubinet, M., Heinesch, B., Du Jardin, P. and Delaplace, P. (2018) Decrease in the photosynthetic performance of temperate grassland species does not lead to a decline in the gross primary production of the ecosystem. *Front. Plant Sci.* **9**, 1–16. https://doi.org/10.3389/fpls.2018.00067.

17. King, R. R., Lawrence, C. H. and Gray, J. A. (2001) Herbicidal Properties of the Thaxtomin Group of Phytotoxins. *J. Agric. Food Chem.* **49**, 2298–2301. https://doi.org/10.1021/jf0012998.

18. Xiao, L., Du, F., Zhou, Y. and Wang, Z. (2018) Isolation of chlamydosporin indole derivative from Fusarium chlamydosporum QJP1 fermentation useful as herbicide. CN 2018-10125578.

19. Tice, C. M. (2001) Selecting the right compounds for screening: Does Lipinski's rule of 5 for pharmaceuticals apply to agrochemicals? *Pest Manag. Sci.* **57**, 3–16. https://doi.org/10.1002/1526-4998(200101)57:1<3::AID-PS269>3.0.CO;2-6.

20. Clarke, E. D. and Delaney, J. S. (2006) Physical and Molecular Properties of Agrochemicals: An Analysis of Screen Inputs, Hits, Leads, and Products. *Chim. Int. J. Chem.* **57**, 731–734. https://doi.org/10.2533/000942903777678641.

21. Szigeti, Z., Tóth, E. and Paless, G. (1982) Mode of action of photosynthesis inhibiting 4-hydroxy-benzonitriles containing nitro group. *Photosynth. Res.* **3**, 347–356. https://doi.org/10.1007/BF00034115.

22. Varejão, J. O. S., Barbosa, L. C. A., Varejão, E. V. V., Maltha, C. R. A., King-Díaz, B. and Lotina-Hennsen, B. (2014) Cyclopent-4-ene-1,3-diones: A new class of herbicides acting as potent photosynthesis inhibitors. *J. Agric. Food Chem.* **62**, 5772–5780. https://doi.org/10.1021/jf5014605.

23. Bajwa, A. A., Ullah, A., Farooq, M., Chauhan, B. S. and Adkins, S. (2019) Chemical control of parthenium weed (Parthenium hysterophorus L.) in two contrasting cultivars of rice under direct-seeded conditions. *Crop Prot.* **117**, 26–36. https://doi.org/https://doi.org/10.1016/j.cropro.2018.11.009.

24. Deligios, P. A., Carboni, G., Farci, R., Solinas, S. and Ledda, L. (2019) The influence of herbicide underdosage on the composition and diversity of weeds in oilseed rape (Brassica napus L. var. oleifera D.C.) mediterranean fields. *Sustain.* **11**, 1653. https://doi.org/10.3390/su11061653.

25. Musiol, R., Tabak, D., Niedbala, H., Podeszwa, B., Jampilek, J., Kralova, K., Dohnal, J., Finster, J., Mencel, A. and Polanski, J. (2008) Investigating biological activity spectrum for novel quinoline analogues 2: Hydroxyquinolinecarboxamides with photosynthesis-inhibiting activity. *Bioorg. Med. Chem.* **16**, 4490–4499. https://doi.org/https://doi.org/10.1016/j.bmc.2008.02.065.

26. Castelo-Branco, P. A., Dos Santos, F. J. L., Rubinger, M. M. M., Ferreira-Alves, D. L., Piló-Veloso, D., King-Díaz, B. and Lotina-Hennsen, B. (2008) Inhibition and uncoupling of photosynthetic electron transport by diterpene lactone amide derivatives. *Zeitschrift fur Naturforsch. - Sect. C J. Biosci.* **63**, 251–259. https://doi.org/10.1515/znc-2008-3-415.

27. Dolezal, M., Zitko, J., Osicka, Z., Kunes, J., Vejsova, M., Buchta, V., Dohnal, J., Jampilek, J. and Kralova, K. (2010) Synthesis, antimycobacterial, antifungal and photosynthesis-inhibiting activity of chlorinated N-phenylpyrazine-2-carboxamides. *Molecules* **15**, 8567–8581. https://doi.org/10.3390/molecules15128567.

28. Rashotte, A. M., Brady, S. R., Reed, R. C., Ante, S. J. and Muday, G. K. (2000) Basipetal Auxin Transport Is Required for Gravitropism in Roots of Arabidopsis. *Plant Physiol.* **122**, 481 LP – 490. https://doi.org/10.1104/pp.122.2.481.

29. Cojocaru, O. A., Shamshina, J. L., Gurau, G., Syguda, A., Praczyk, T., Pernak, J. and Rogers, R. D. (2013) Ionic liquid forms of the herbicide dicamba with increased efficacy and reduced volatility. *Green Chem.* **15**, 2110–2120. https://doi.org/10.1039/C3GC37143C.

30. Wang, T., Bing, G., Zhang, X., Qin, Z., Yu, H., Qin, X., Dai, H., Miao, W., Wu, S. and Fang, J. (2010) Synthesis and herbicidal activities of 2-cyano-3-benzylaminoacrylates containing thiazole moiety. *Bioorg. Med. Chem. Lett.* **20**, 3348–3351. https://doi.org/https://doi.org/10.1016/j.bmcl.2010.04.027.

31. Ma, H.-J., Li, Y.-H., Zhao, Q.-F., Zhang, T., Xie, R.-L., Mei, X.-D. and Ning, J. (2010) Synthesis and Herbicidal Activity of Novel N-(2,2,2)-Trifluoroethylpyrazole Derivatives. *J. Agric. Food Chem.* **58**, 4356–4360. https://doi.org/10.1021/jf9042166.

32. Wang, D.-W., Lin, H.-Y., Cao, R.-J., Chen, T., Wu, F.-X., Hao, G.-F., Chen, Q., Yang, W.-C. and Yang, G.-F. (2015) Synthesis and Herbicidal Activity of Triketone–Quinoline Hybrids as Novel 4-Hydroxyphenylpyruvate Dioxygenase Inhibitors. *J. Agric. Food Chem.* **63**, 5587–5596. https://doi.org/10.1021/acs.jafc.5b01530.

33. Kakwani, M. D., Suryavanshi, P., Ray, M., Rajan, M. G. R., Majee, S., Samad, A., Devarajan, P. and Degani, M. S. (2011) Design, synthesis and antimycobacterial activity of cinnamide derivatives: A molecular hybridization approach. *Bioorg. Med. Chem. Lett.* **21**, 1997–1999. https://doi.org/https://doi.org/10.1016/j.bmcl.2011.02.022.

34. Barbosa, T. P., Sousa, S. C. O., Amorim, F. M., Rodrigues, Y. K. S., de Assis, P. A. C., Caldas, J. P. A., Oliveira, M. R. and Vasconcellos, M. L. A. A. (2011) Design, synthesis and antileishmanial in vitro activity of new series of chalcones-like compounds: A molecular hybridization approach. *Bioorg. Med. Chem.* **19**, 4250–4256. https://doi.org/https://doi.org/10.1016/j.bmc.2011.05.055.

35. Karthikeyan, C., Solomon, V. R., Lee, H. and Trivedi, P. (2013) Design, synthesis and biological evaluation of some isatin-linked chalcones as novel anti-breast cancer agents: A molecular hybridization approach. *Biomed. Prev. Nutr.* **3**, 325–330.

https://doi.org/https://doi.org/10.1016/j.bionut.2013.04.001.

36. Gündüz, M. G., Tahir, M. N., Armaković, S. J. S., Özkul Koçak, C. and Armaković, S. J. S. (2019) Design, synthesis and computational analysis of novel acridine-(sulfadiazine/sulfathiazole) hybrids as antibacterial agents. *J. Mol. Struct.* **1186**, 39–49. https://doi.org/https://doi.org/10.1016/j.molstruc.2019.03.010.

37. Reddyrajula, R. and Dalimba, U. (2019) Quinoline–1,2,3-triazole Hybrids: Design and Synthesis through Click Reaction, Evaluation of Anti-Tubercular Activity, Molecular Docking and In Silico ADME Studies. *ChemistrySelect* **4**, 2685–2693. https://doi.org/10.1002/slct.201803946.

38. Raker, J., Wang, Y., Pechulis, A. D., Haber, J. C., Lynch, M. A. and Spring, S. L. (2012) Synthesis of novel benzo[b]pyrazolo[1,5]diazepines. *J. Heterocycl. Chem.* **49**, 221–226. https://doi.org/10.1002/jhet.878.

39. Czeskis, B. A. and Wheeler, W. J. (2005) Synthesis of β3 adrenergic receptor agonist LY377604 and its metabolite 4-hydroxycarbazole, labeled with carbon-14 and deuterium. *J. Label. Compd. Radiopharm.* **48**, 407–419. https://doi.org/10.1002/jlcr.935.

40. Deorha, D. and Joshi, S. (1961) Notes- Cyclic Products from Hydrazines. I. Nitroindoles, Nitrotetrahydrocarbazoles, Nitroindolenines and Nitrotetrahydrocarbazolenines. *J. Org. Chem.* **26**, 3527–3530. https://doi.org/10.1021/jo01067a614.

41. Hadida Ruah, Sara S.; Grootenhuis, Peter D.J.; Van Goor, Frederick; Zhou, Jinglan; Bear, Brian; Miller, Mark T.; McCartney, Jason; Numa, M. M. J. (2007) Modulators of ATP-binding cassette transporters. 1–208.

42. Perkin, W. H. and Plant, S. G. P. (1923) LXXXI.—Derivatives of tetrahydrocarbazole. Part II. *J. Chem. Soc. Trans.* **123**, 676–695. https://doi.org/10.1039/CT9232300676.

43. Collar, W. M. and Plant, S. G. P. (1926) CIX.—Derivatives of tetrahydrocarbazole. Part V. Carboxylic acids. *J. Chem. Soc.* **129**, 808–810. https://doi.org/10.1039/JR9262900808.

44. Brown, U. M., Carter, P. H. and Tomlinson, M. (1958) 374. Formyl compounds. Part II. *J. Chem. Soc.* 1843–1849. https://doi.org/10.1039/JR9580001843.

45. Miller, W H; Newlander, K A; Seefeld, M A; Uzinskas, I N; Dewolf, W E Jr; Jakas, D. R. (2002) Fab I Inhibitors.

46. Allouche, A. (2012) Software News and Updates Gabedit — A Graphical User Interface for Computational Chemistry Softwares. *J. Comput. Chem.* **32**, 174–182. https://doi.org/10.1002/jcc.

47. Nain-Perez, A., Barbosa, L. C. A., Maltha, C. R. A., Giberti, S. and Forlani, G. (2017) Tailoring Natural Abenquines to Inhibit the Photosynthetic Electron Transport through Interaction with the D1 Protein in Photosystem II. *J. Agric. Food Chem.* **65**, 11304–11311. https://doi.org/10.1021/acs.jafc.7b04624.

48. Brozell, S. R., Mukherjee, S., Balius, T. E., Roe, D. R., Case, D. A. and Rizzo, R. C. (2012) Evaluation of DOCK 6 as a pose generation and database enrichment tool. *J. Comput. Aided. Mol. Des.* **26**, 749–773. https://doi.org/10.1007/s10822-012-9565-y.

49. Oukarroum, A., El Madidi, S. and Strasser, R. J. (2016) Differential heat sensitivity index in barley cultivars (Hordeum vulgare L.) monitored by chlorophyll a fluorescence OKJIP. *Plant Physiol. Biochem.* **105**, 102–108. https://doi.org/https://doi.org/10.1016/j.plaphy.2016.04.015.

50. Dai, Y., Yuan, L., Zhang, S., Wang, J., Xie, S., Zhao, M., Chen, G., Sun, R. and Wang, C. (2019) Comprehensive evaluation for cold tolerance in wucai (brassica campestris l.) by the performance index on an absorption basis (PIabs). *Agronomy* **9**, 1–18. https://doi.org/10.3390/agronomy9020061.

51. Paoli, L. and Landi, M. (2013) The photosynthetic performance of sterile and fertile sporophytes in a natural population of the fern Dryopteris affinis. *Photosynthetica* **51**, 312–316. https://doi.org/10.1007/s11099-013-0022-5.

52. Chen, S., Kang, Y., Zhang, M., Wang, X., Strasser, R. J., Zhou, B. and Qiang, S. (2015) Differential sensitivity to the potential bioherbicide tenuazonic acid probed by the JIP-test based on fast

chlorophyll fluorescence kinetics. *Environ. Exp. Bot.* **112**, 1–15. https://doi.org/https://doi.org/10.1016/j.envexpbot.2014.11.009.

53. Kalaji, H. M., Schansker, G., Ladle, R. J., Goltsev, V., Bosa, K., Allakhverdiev, S. I., Brestic, M., Bussotti, F., Calatayud, A., Dąbrowski, P., Elsheery, N. I., Ferroni, L., Guidi, L., Hogewoning, S. W., Jajoo, A., Misra, A. N., Nebauer, S. G., Pancaldi, S., Penella, C., Poli, D., Pollastrini, M., Romanowska-Duda, Z. B., Rutkowska, B., Serôdio, J., Suresh, K., Szulc, W., Tambussi, E., Yanniccari, M. and Zivcak, M. (2014) Frequently asked questions about in vivo chlorophyll fluorescence: practical issues. *Photosynth. Res.* **122**, 121–158. https://doi.org/10.1007/s11120-014-0024-6.

54. de Carvalho, A. C., Salvador, J. P., Pereira, Thais de M. , Ferreira, P. H. A., Lira, J. C. S. and Veiga, T. A. M. (2016) Fluorescence of Chlorophyll a for Discovering Inhibitors of Photosynthesis in Plant Extracts. *Am. J. Plant Sci.* **07**, 1545–1554.

55. McConnell, I., Li, G. H. and Brudvig, G. W. (2010) Energy Conversion in Natural and Artificial Photosynthesis. *Chem. Biol.* **17**, 434–447. https://doi.org/10.1016/j.chembiol.2010.05.005.

56. Avram, S., Funar-Timofei, S., Borota, A., Chennamaneni, S. R., Manchala, A. K. and Muresan, S. (2014) Quantitative estimation of pesticide-likeness for agrochemical discovery. *J. Cheminform.* **6**, 42. https://doi.org/10.1186/s13321-014-0042-6.

57. Sobolev, V. and Edelman, M. (1995) Modeling the quinone-B binding site of the photosystem-II reaction center using notions of complementarity and contact-surface between atoms. *Proteins Struct. Funct. Bioinforma.* **21**, 214–225. https://doi.org/10.1002/prot.340210304.

58. Takahashi, R., Hasegawa, K., Takano, A. and Noguchi, T. (2010) Structures and Binding Sites of Phenolic Herbicides in the QB Pocket of Photosystem II. *Biochemistry* **49**, 5445–5454. https://doi.org/10.1021/bi100639q.

59. Guo, Y., Cheng, J., Lu, Y., Wang, H., Gao, Y., Shi, J., Yin, C., Wang, X., Chen, S., Strasser, R. J. and Qiang, S. (2020) Novel Action Targets of Natural Product Gliotoxin in Photosynthetic Apparatus

. *Front. Plant Sci.* **10**, 1688.

FIGURE CAPTIONS

Figure 1. Design of amide or nitro indole derivatives from known herbicidal activity compounds.

Figure 2. Performance Index (PI_{abs}) of spinach leaf discs subjected to **15a-d**, **16a-d**, **20a-b** and **21a-b** (100 μM). (*) and (**) indicate significant difference from control (DMSO) with $p < 0.05$ and $p < 0.01$, respectively.

Figure 3. Radar plots of the effects of (A) **15a,** (B) **15b** and (C) **21b** on Chl *a* fluorescence parameters calculated from the OJIP curve in spinach sheet discs at 50 μM and 100 μM.

Figure 4. Performance Index (PI_{abs}) of (A) *I. grandifolia* at 72 hours, (B) *S. alata* at 72 hours and (C) *S. rhombifolia* at 1 hour treated with **15a-b** and **21b** (50 μM and 100 μM). (*) and (**) indicate significant difference from control (DMSO) with $p < 0.05$ and $p < 0.01$, respectively.

Figure 5. Radar plots of the effects of **15a-b** and **21b** on (A) *I. grandifolia* at 72 hours, (B) *S. alata* at 72 hours and (C) *S. rhombifolia* at 1 hour on Chl *a* fluorescence parameters calculated from the OJIP curve at 50 μM.

Figure 6. Plant length and dry biomass of (A) *I. grandifolia,* (B) *S. alata* and (C) *S. rhombifolia* after 10 days of treatment with **15a-b** and **21b** at 50 and 100 μM. (*) and (**) indicate significant difference from control (DMSO) with $p < 0.05$ and $p < 0.01$, respectively.

Figure 7. Binding models of **15a** (**A**) and **15b** (**B**) with the pocket site of PSII from *S. oleracea* (PDB code: 3JCU).

SCHEME CAPTIONS

Scheme 1. Synthesis of compounds **15a-d** and 1**6a-d**.

Scheme 2. Synthesis of compounds **21a-b**.

13a, R_1= Cl, R_2= NO_2
13b, R_1= NO_2, R_2= Cl

14a, R_1= Cl, R_2= NO_2
14b, R_1= NO_2, R_2= Cl

15a, R_1= Cl, R_2= NO_2, R_3= R_4= -$(CH_2)_4$-
15b, R_1= Cl, R_2= NO_2, R_3= R_4= CH_3
15c, R_1= NO_2, R_2= Cl, R_3= R_4= -$(CH_2)_4$-
15d, R_1= NO_2, R_2= Cl, R_3= R_4= CH_3

16a, R_1= Cl, R_2= NHAc, R_3= R_4= -$(CH_2)_4$-
16b, R_1= Cl, R_2= NHAc, R_3= R_4= CH_3
16c, R_1= NHAc, R_2= Cl, R_3= R_4= -$(CH_2)_4$-
16d, R_1= NHAc, R_2= Cl, R_3= R_4= CH_3

Reagents and conditions: (**a**) $NaNO_{2(aq)}$, HCl, 0ºC; (**b**) $SnCl_2.2H_2O$, HCl, 0ºC; (**c**) cyclohexanone or butanone, H_2SO_4, H_2O, reflux; (**d**) $ZnCl_2$, HAc, reflux; (**e**) $SnCl_2.2H_2O$, AcOEt, r.t.; (**f**) Ac_2O, NaOAc, HAc, r.t.

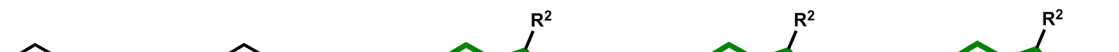

17

18

17a, R^1=R^2= -$(CH_2)_4$-
17b, R^1=R^2= CH_3

18a, R^1=R^2= -$(CH_2)_4$-
18b, R^1=R^2= CH_3

19a, R^1=R^2= -$(CH_2)_4$-
19b, R^1=R^2= CH_3

Reagents and conditions: (**a**) 2-butanone or cyclohexanone, HAc, reflux; (**b**) H_2SO_4, EtOH, reflux; (**c**) $MeNH_2$, EtOH, r.t.

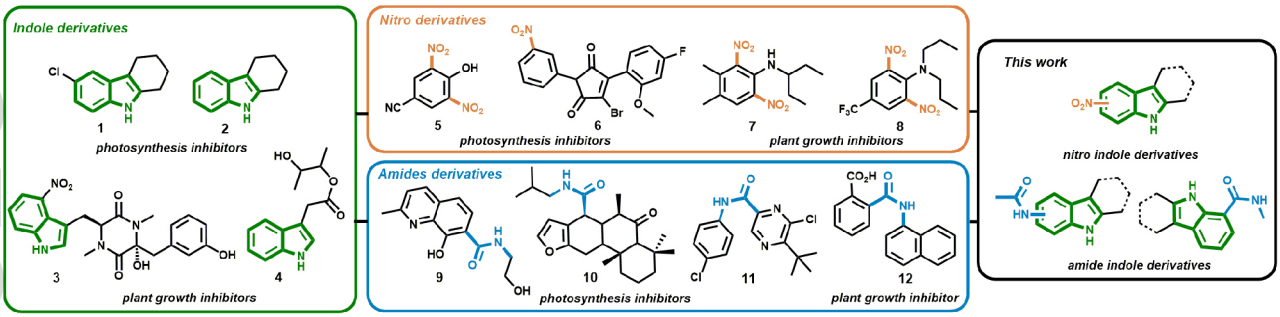

php_13295_f1.jpg

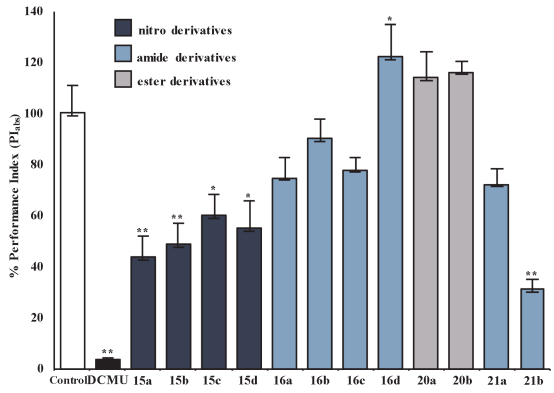

php_13295_f2.tif

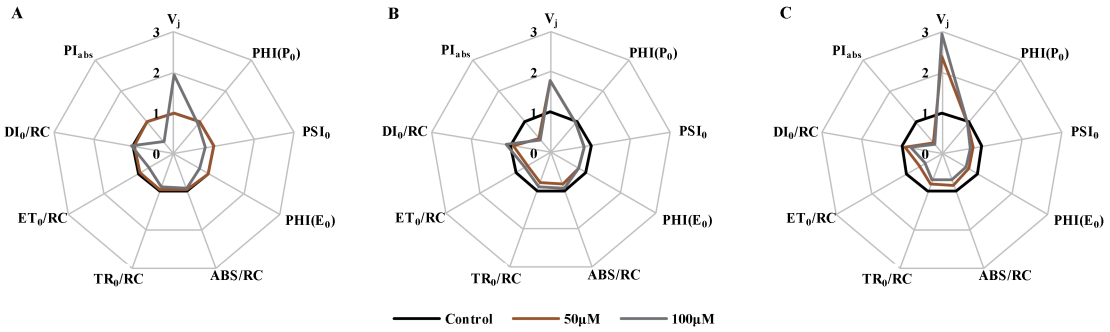

php_13295_f3.tif

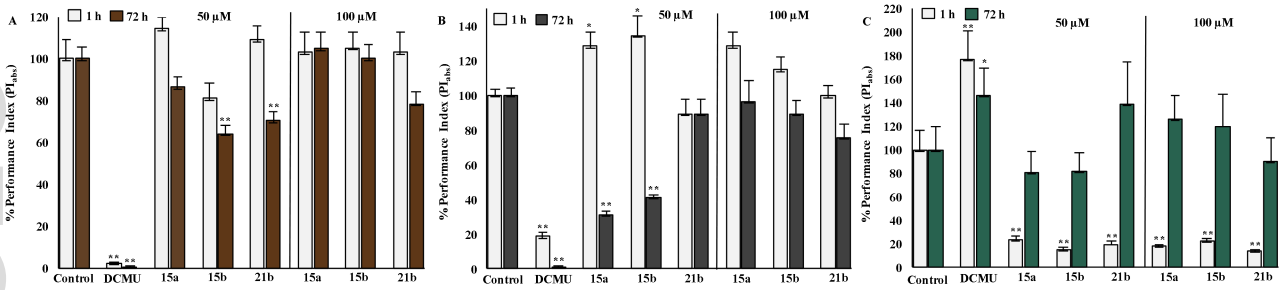

php_13295_f4.tif

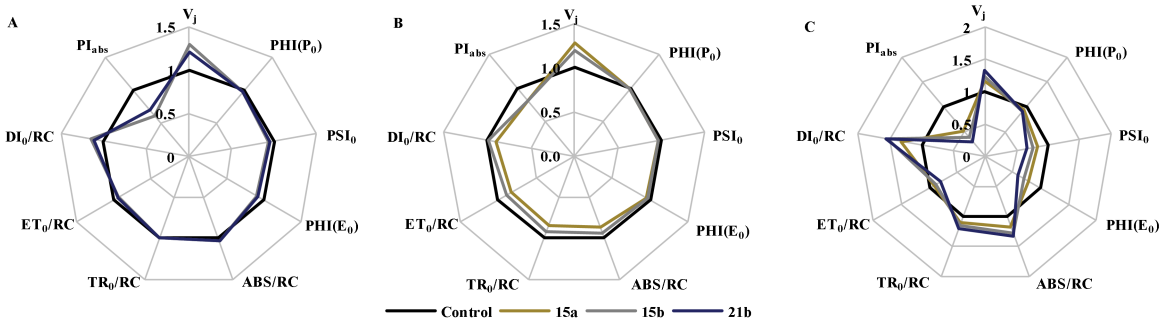

php_13295_f5.tif

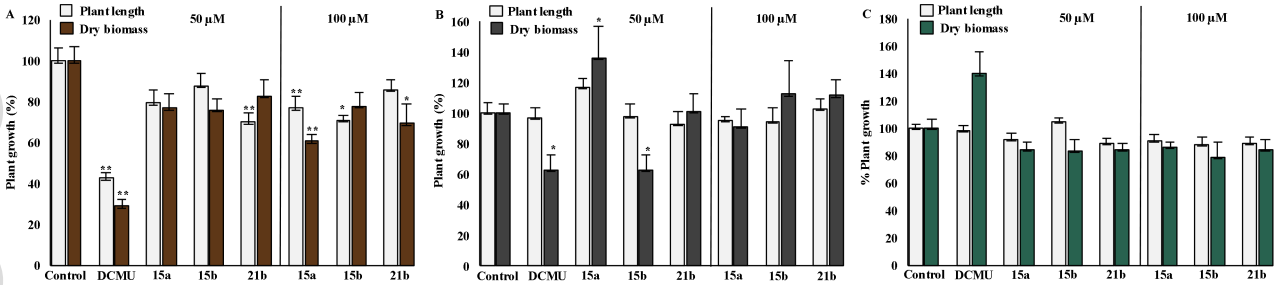

php_13295_f6.tif

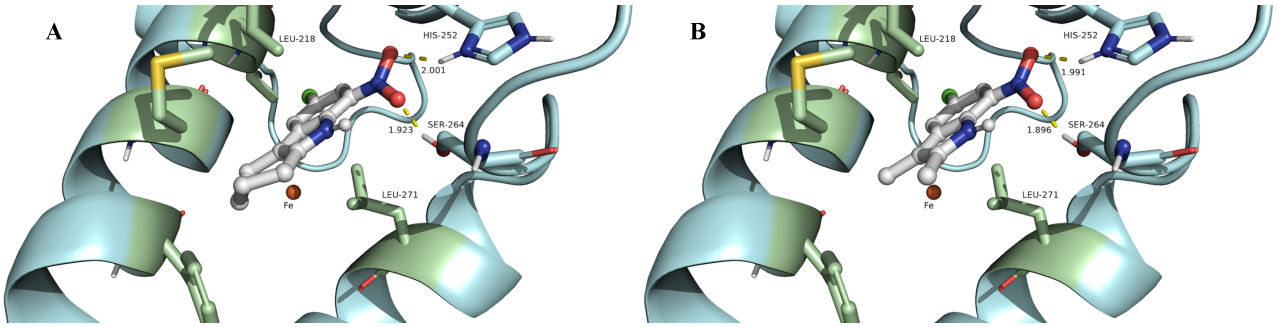

php_13295_f7.tif